

# FLAT SLAB BRIDGE MODEL FOR PERMIT LOAD ANALYSIS

PATRYK J. WOLERT, *e-mail: pjw0008@auburn.edu*

ANDRZEJ S. NOWAK

J. MICHAEL STALLINGS

Department of Civil Engineering, Auburn University, Auburn Alabama, USA

**Abstract:** Alabama Department of Transportation (ALDOT) has an existing, eleven-span flat slab reinforced concrete bridge that was built in 1915 for which there are no construction drawings or other available data. The goals of this research are to rate the bridge and provide a model for permit load analysis. ALDOT can then use this model to provide permits for non-standard trucks to travel over this bridge. Field measurements were taken using specialized equipment to assess the dimensions including span length, width, location and size of reinforcement, thickness of the slab, thickness of concrete cover, and compressive strength of concrete. The collected data were analyzed and treated as input data to determine a preliminary load carrying capacity of the slab. An advanced Finite Element Method (FEM) program ABAQUS was used to develop a 3-D model of the slab. The behavior of the bridge slab was then verified by load test, with the load applied using one and two 380-kN 3-axle trucks. The load test results were used to further improve the Finite Element (FE) Model and in particular, to estimate an improved value of bridge rating and the effective slab width. Proposed newly developed adjustments in the selection of input data in AASHTOWare software result in a more rational evaluation and rating of the considered bridge.

**Keywords:** nondestructive bridge testing, flat slab bridge, reinforced concrete, existing structure evaluation, rating factor, nonlinear material model, finite element model of the bridge, live-load testing

## 1. Introduction

Alabama Department of Transportation (ALDOT) has an existing, eleven-span flat slab reinforced concrete bridge over Barnes Slough and Jenkins Creek on the southbound side of Montgomery, Alabama (Fig. 1) for which there are no construction drawings or other details that can be used to perform a load rating of the structure.

Currently the bridge carries unrestricted traffic. This is allowed by AASHTO's *The Manual for Bridge Evaluation* [1] in cases where a reinforced concrete bridge of unknown details has carried unrestricted traffic without developing signs of distress. Because the structural details of the bridge are unknown, ALDOT cannot perform an analysis to justify issuing a permit to any overweight, non-standard trucks.

## 2. Considered structure

The considered structure is an 11-span flat slab reinforced concrete bridge (Fig. 1), with no existing technical drawings nor other details. The construction year was established as 1915 from a report of the state [2], and ALDOT's records showed that it was widened by approximately 1.20 m in 1930. Visual inspection of the bridge indicates that the bridge was widened twice. It was not established when the second widenings were added. Also, the existence of some cracks on the sides of the slab near the supports were indicative of shrinkage or temperature cracking in the concrete, but there were no significant signs of flexural or shear cracking, nor evidence of anchorage or bond failure.



Fig. 1. Side view of the bridge

All 11 spans are equal and the center-to-center span length is 6.65 m, while the total width is 9.56 m. Pier wall thickness is 0.61 m. Total cross section width for each span of the bridge consists of four segments: the original one and three additions. The width of the oldest segment (segment 3) is 5.49 m.

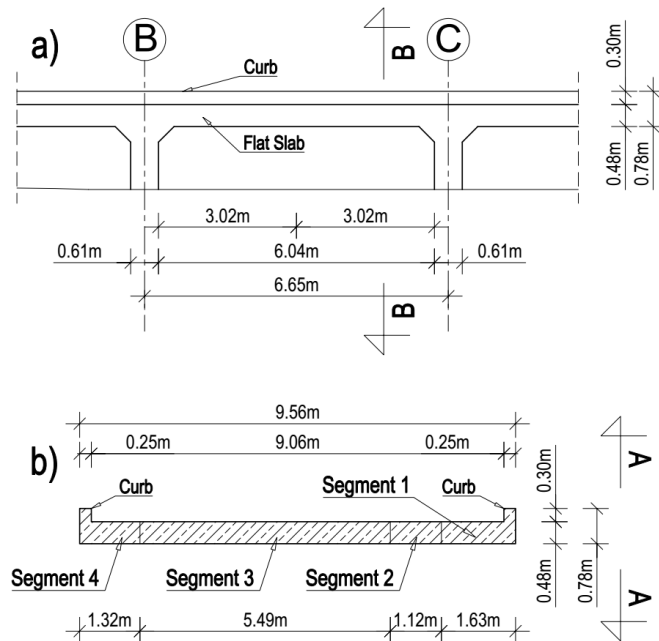


Fig. 2. Detailed drawings of the bridge, a) elevation view A–A, b) cross section B–B

First, the bridge was widened by 1.12 m on the East side (segment 2) – Fig. 2. Then it was widened on both sides by 1.63 m on the East side (segment 1) and 1.32 m on the West side (segment 4).

### 3. Field measurements

Field measurements involved detection and measurement of slab's reinforcement and slab thickness measurements. The research team used a thickness measuring device, which uses Ultrasonic Pulse Velocity (UPV) testing and an Advanced Concrete Cover Meter (ACCM) which measures spacing between reinforcing bars and their diameter. These two instruments were used to inspect the bottom of the slab. Top reinforcement was scanned with Ground Penetrating Radar (GPR).

Using the UPV testing device, bottom surfaces of the first and second span were scanned. Measurements of the concrete slab indicated that its thickness can be assumed as 48 cm (Fig. 3).

Bottom surface of the bridge was scanned with ACCM, an instrument using electromagnetic pulse induction technology. The ACCM detected locations of the bottom rebars, measured their diameters and cover thickness. A summary of the bottom reinforcement found, is presented in Table 1.

Table 1. Details of the bottom reinforcing bars

Segment No.	Rebar size [mm]	Cover [mm]	Number of rebars in segment
1	Φ25	32	10
2	Φ22	32	9
3	Φ25	32	53
4	Φ25	32	7

The cover of 32 mm was chosen as it conservatively represents maximum clear cover of some instances. To confirm ACCM's reading in two segments the reinforcing bars were exposed. Accuracy of detection and measuring capabilities were confirmed to be good, and interestingly, the exposed rebars turned out to be cupped. AASHTO Manual [1] recommends the yield strength of steel of 227 MPa for unknown reinforcing steels built prior to 1954.



Fig. 3. Cylindrical concrete sample drilled (1in. = 25.4 mm)

Top surface of the bridge is a 5 cm layer of asphalt, and it was investigated using the GPR. The GPR provided information on the top reinforcement distribution and detected transverse cracks over the support locations. One concrete sample was drilled thru a top reinforcing bar and gave the information on top rebars size – Φ12, Fig. 3.

From these findings it was concluded that the bridge was reinforced as if it is a series of simple spans, and in subsequent load capacity calculations simple support conditions were assumed with top reinforcement neglected entirely.

At least three different concrete mixes were used in the bridge. Due to restrictions on the number of cores that could be taken, only three concrete samples are available. One core was drilled in segment 3 (Fig. 2), over the support, in the oldest concrete. Additional two cores were taken from segment 1 with the newest concrete, at over support and mid-span locations.

Concrete cylinder compressive strength values obtained in ALDOT's material laboratory are presented in Table 2. For superstructure components constructed prior to 1959 AASHTO Manual [1] recommends a minimum compressive strength value of 17.2MPa, which turned out to be under conservative for segment 1.

Table 2. Compressive test results for concrete cores

Sample	1	2	3
Compressive Strength [MPa]	23.0	13.4	12.1
Location	Original Segment 3 – over support	East Segment 1 – over support	East Segment 1 – midspan

#### 4. Bridge ratings

The bridge load ratings are indispensable for determining maintenance needs, assuring public safety, scheduling retrofit or replacement elements, and for assessing overload permits. General Rating Factor (RF) equation, expressing how much live load can be superimposed on the bridge, is as follows:

$$RF = \frac{C - D}{L(1 + I)} \quad (1)$$

where:  $C$  – Load carrying capacity,  $D$  – Dead Load Effect,  $L$  – Live Load Effect,  $I$  – Impact Factor.

State Departments of Transportation use Load Factor Ratings (LFR) to evaluate bridges in their inventory, which is a concept according to AASHTO Standard Spec [3]. LFR has very similar formula as the one shown in equation (1), the only difference are load factors in equation (2).

$$LFR = \frac{C - A_1 D}{A_2 L(1 + I)} \quad (2)$$

where:  $A_1$  – Factor for Dead Load,  $A_2$  – Factor for Live Load.

LFRs are specified for two levels, inventory and operating. The inventory rating corresponds to design of new structures according to AASHTO [3] and the factor  $A_1$  is equal to 1.30 and  $A_2$  is 2.17. For an operating rating the factors  $A_1$  and  $A_2$  are equal to 1.30 and are used for evaluation of an existing structure. According to [1] and [3] impact factor is 0.30.

For the flat slab bridges a value of effective slab width is needed to perform the rating calculations. AASHTO's [3] effective width carries one line of wheels and is defined by formula below

$$E = 1.22 + 0.06S \leq 2.13 \text{ m} \tag{3}$$

where:  $E$  – Effective width with a maximum value of 2.13 m. Lane loads are distributed over a width of  $2E$ ;  $S$  – For simple spans the span length shall be the distance center-to-center of supports but not to exceed clear span plus thickness of slab (m).

For the considered structure effective width calculated with equation (3) is 1.62 m and it carries one line of wheels. For this two-lane bridge an upper value of effective width is the quarter of the total width of the bridge which is 2.39 m.

AASHTO [1] has a series of standard trucks that are commonly used for rating bridges. These trucks are a good representation of the actual traffic. Load configurations for two chosen vehicles are presented in Fig. 4 and 5, for an AASHTO TriAxle truck (Fig. 4) and for ALDOT’s LC-5 Test truck (Fig. 5).

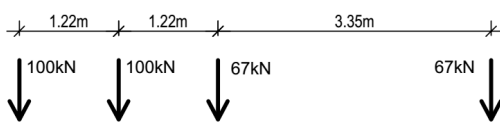


Fig. 4. Axle Weights and axle spacing of AASHTO’s TriAxle truck

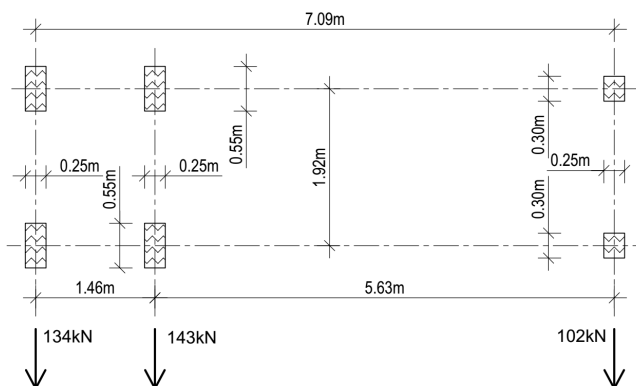


Fig. 5. Axle Weights and axle spacing of ALDOT’s LC-5 test truck

Collected data enabled researches to perform rating calculations and the lowest values of RFs were obtained for these two selected vehicles. Therefore, these two types of trucks are considered in further analysis.

### 5. Permit load model

Permit Load Model developed for ALDOT is a model of simply supported beam with dimensions as described in previous sections of this paper and material parameters as recommended by AASHTO [1]. The purpose of such model development are ease of application in AASHTOWare software which is used by ALDOT, compatibility with AASHTO provisions and recommendations [1, 3] as well as general simplicity and accesability for practitioners. The only parameter which is subjected to adjustments is the effective width. To perform load rating analysis, the most conservative assumptions regarding material properties and structural details of the reinforcement are considered. This was captured in the Final Element (FE) Model of the bridge and is presented in the following sections of this paper. FE Model aided ratings

were compared with those obtained through AASHTO procedure and resulted in adjustments in effective width selection.

A series of LFRs calculations were performed for two selected models. Original Segment model with reinforcement of the oldest segment number 3 and East Segment model with reinforcement corresponding to the rebar distribution in segments number 1 and 2 (Fig. 2, Table 1). Rating Factors were calculated for both, upper and lower bounds of the effective width for both models. Results of load rating calculations are presented in the table below.

Table 3. LFRs for east and original segment models

Model	East Segment		East Segment		Original Segment		Original Segment	
	Effective width, $E$ [m]		Effective width, $E$ [m]		Effective width, $E$ [m]		Effective width, $E$ [m]	
Effective width, $E$ [m]	1.62		2.39		1.62		2.39	
Vehicle\LFR Level*	O	I	O	I	O	I	O	I
LC-5	0.66	0.40	1.37	0.82	1.56	0.94	2.28	1.37
TriAxle	0.64	0.38	1.31	0.78	1.50	0.90	2.20	1.32

\* O – Operating Level, I – Inventory Level

The load ratings in Table 3 are surprisingly low, in spite of conservative assumptions and calculation procedure.

## 6. Live-load tests

The bridge was subjected to live-load tests with usage of two ALDOT's LC-5 Test Trucks (Fig. 4 and 6) weighing 38.6t each. Tests included strain and deflection measurements at sensor mounting locations.

All the strain transducers were placed at midspan locations under first two spans. Four deflection measuring LVDTs were collecting data during the tests. Maximum longitudinal strain value recorded during the tests was  $34\mu\epsilon$  for a sensor mounted 10 cm off the East edge and two trucks placed side-by-side. Maximum deflection of 0.60 mm was recorded for two trucks side-by-side on West edge of the bridge. It was concluded that the bridge, although consists of four different width segments, behaves symmetrically. Results of static tests further served for calibration of a Finite Element (FE) Model of the bridge.



Fig. 6. Example of the load configurations (1) two trucks side-by-side (2) one truck 0.30 m away from curb

## 7. Finite element model

A three dimensional FE Model of a single span (Fig. 7), the first span at the south end of the bridge, was developed in Simulia Abaqus 6.14 FE Software [4]. This section presents development of the FE Model of the bridge and presents results of the calibration.

Findings from field measurements, as well as relative similarity of the measured deflections and strains for both spans tested led to the conclusion that the model of one span will best reflect the behavior of the bridge. The model was developed using solid and beam elements, which allowed for a detailed investigation of local stress and strain distributions as well as overall bridge behavior.

Preliminary analysis showed that the bridge was capable of carrying two LC-5 trucks with Gross Vehicle Weight  $GVW = 38.6$  t each during live load tests. After the load tests were performed the FE model was calibrated to have the same response as the real structure.

The model contains upper pieces of the piers, slab, bottom reinforcing bars, and curbs of dimensions as shown in Fig. 2. The curbs have cross-sectional dimensions of  $20 \times 25$  cm. Four different width segments, fully bonded with each other, create each of the simple span slabs.

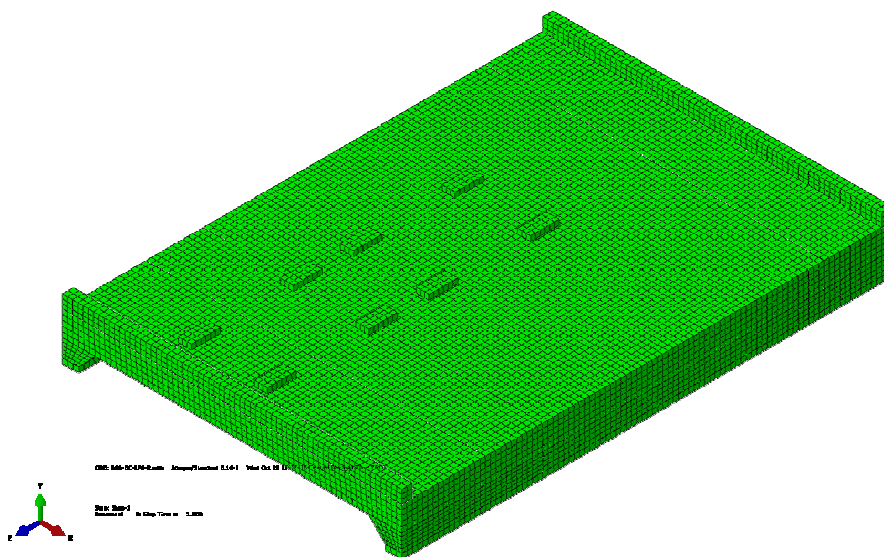


Fig. 7. Isometric view of the FE model of the bridge. ALDOT test trucks footprint pattern presented

### Element types

Among the various element types available in the Finite Element Method (FEM) only selected elements are presented. The concrete elements – curbs, slab segments and piers were modelled with 8-noded linear brick elements with reduced integration C3D8R [4]. Reduced integration element was chosen due to its computational cost, which is smaller than for a full-integration element. The element type used for reinforcing bars is a 2-node linear beam element B31 [4]. The advantage of the beam over widely used link elements in FE modelling of reinforcement is its ability to act in compression as well as in tension. Both element types selected, C3D8R and B31, have six degrees of freedom at each node – translations and rotations in the nodal x, y, and z directions. For a stress/displacement simulations the degrees of freedom are the translations for brick elements, and for the beam elements rotations and translations at each node.

The reinforcing bars were modelled as in the real structure (Table 1), the reinforcement is embedded into slab. From the numerical method point of view an embedded rebar acts as fully bonded with concrete slab. Although, the rebars occur in all of the concrete elements they were modelled in the slabs only. Modelling of the reinforcement in other elements was not critical.

The mesh study showed that the most effective mesh size, in terms of accuracy and computing time, is  $10 \times 10 \times 9.7$  cm for the brick elements and 10 cm of length for the beam elements.

### Numerical material models

To develop numerical material models all collected data with available literature was reviewed. The FEM requires specification of material parameters such as modulus of elasticity, Poisson's ration and stresses with corresponding strains in non-linear stress ranges. Two non-linear material models, Concrete Damage Plasticity (CDP) for concrete and elasto-plastic for steel, were implemented into the FE model. Material non-linearity is justified by need for accurate stress investigation for loads causing concrete cracking and non-linear material behavior.

### Concrete material model

The CDP model available in Abaqus software requires parameters are associated with simplified Drucker-Prager concrete strength hypothesis. Description and selection of these parameters are available in [4] and [5]. In addition to those, CDP model requires stress-strain data within inelastic region for compressive and tensile behavior. These can be determined from strain-stress curve. Due to the lack of accurate stress-strain data for the concrete samples taken, the relationship curves had to be approximated as described below.

ACI 318-14 [6] provides the formula, where modulus of elasticity,  $E$  is a function of concrete compressive strength,  $f'_c$ . During the calibration process it was found out that Eurocode formula [7] for the modulus of elasticity (4) adopted to the FE Model produce values of strains and deflections which match the measured values better. The Eurocode formula for modulus of elasticity was used and is presented below

$$E_c = 22(f'_c)^{1/3} \quad (4)$$

where:  $E_c$  – Initial Modulus of Elasticity (GPa),  $f'_c$  – Compressive Strength of Concrete (MPa).

The compressive stress-strain relationship curves were established with the Desayi and Kirshnan [8] equation

$$\sigma_c = \frac{E \varepsilon_c}{1 + \left(\frac{\varepsilon_c}{\varepsilon_0}\right)^2} \quad (5)$$

where:  $\sigma_c$  – Compressive Stress,  $\varepsilon_c$  – Compressive Strain,  $\varepsilon_0$  – Strain at maximum Stress,  $E$  – Initial tangent modulus, assumed to be twice the secant modulus at maximum stress  $\sigma_{max}$ .

It is assumed that numerical concrete material models perform linearly up the stress of  $0.4f'_c$ .

The tensile stress-strain relationship was developed using the Wang and Hsu formula [9] which most accurately describes concrete tension stiffening

$$\left\{ \begin{array}{l} \sigma_t = E_c \varepsilon_t \quad \text{if } \varepsilon_t \leq \varepsilon_{cr} \\ \sigma_t = f_c' \left( \frac{\varepsilon_{cr}}{\varepsilon_t} \right)^{0.4} \quad \text{if } \varepsilon_t > \varepsilon_{cr} \end{array} \right. \quad (6)$$

where:  $\sigma_t$  – Tensile Stress,  $\varepsilon_t$  – Tensile Strain,  $\varepsilon_{cr}$  – Cracking Strain.

In order to establish cracking strain the modulus of rupture needs to be known. The AASHTOs’ metric formula [3] was used to establish the tensile strength of the concrete (7).

$$f_r = 0.623 \sqrt{f_c'} \quad (7)$$

where:  $f_r$  – Modulus of Rupture (MPa),  $f_c'$  – Compressive Strength of Concrete (MPa).

Four different compressive strengths of concrete were taken for each of the four segments of the bridge. Using the concrete compressive strengths for each of the slab’s segments, the approximated stress-strain relationships were developed for the compressive and the tensile behavior. The compressive strengths used as well as the values of corresponding modulus of elasticity are shown in the Table 4.

Table 4. Parameters of concrete for each of the slab’s segments.

Segment	4 (West Bound)	3	2	1 (East Bound)
$f_c'$ [MPa]	12.8	23.0	12.1	13.4
$E$ [GPa]	23.7	28.2	23.3	24.0

### Steel material model

Provisions from AASHTO Manual [1] allowed to develop the material model for reinforcing steel bars. The Manual recommends the yield strength of steel of 227 MPa for unknown reinforcing steels built prior to 1954. For assumed modulus of elasticity of 200 GPa the reinforcing bars reach yielding at strain value of 0.1%. The ultimate tensile strength of steel was taken as 380 MPa [10] and assumed to occur at strain of 1.0%. Within the inelastic region the stress-strain relationship is assumed linear for computational stability.

### Boundary conditions and loads

First supporting pier has restrained displacements in Y and Z directions, not restrained displacement in X direction allows it to move in longitudinal direction – parallel to direction of traffic. Second pier has all the displacements restrained. The rotations for both piers are allowed in all the directions. Allowed displacement in Y (vertical) direction at the front and back surfaces of the slab immitates it’s discontinuity due to the transverse cracks detected over the supports (Fig. 7).

Contact conditions specified in the model are as follows: full bond of reinforcing bars with concrete in all segments, full connection to the side surfaces of the adjacent segments, pressure transfer interaction between tire footprint elements and concrete segments. Static wheel loads on the bridge are modelled as flat rigid load transferring plates with a uniform load applied. Load applied to the model was the actual truck used during the live load tests (Fig. 5).

### Results of calibration

The calibrated FE model replicates strains and deflections within acceptable tolerance for the integration points at the same locations as sensors. Maximum offset in the strains is  $12 \mu\epsilon$ , while for deflections it is 0.09 mm. This allowed plotting the values obtained through FE analyses and field test measurements for all the static load patterns. Just one comparison plot for critical load pattern is presented (Fig. 8). FEM values present the actual distribution of longitudinal strains and deflections in the cross-section. Vertical dashed lines indicate the boundaries between the different cross section of segments. West side of the bridge corresponds to the distance along the width of 0 inches, while East side corresponds to the value of 376 inches.

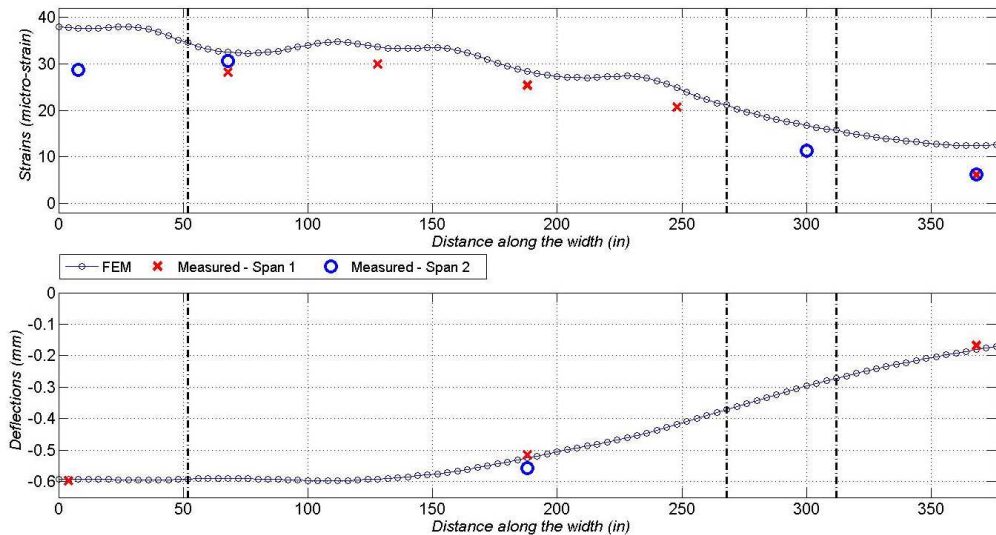


Fig. 8. Comparison plot of Strains and Deflections for the most critical load pattern (1 in. = 2.54 cm)

It is concluded that the model shows an overall good correlation with the measured values. Even though the bridge is a hybrid structure with different widths of slab segments, it responds as if it was homogenous.

### 8. Bridge rating using finite element model

The FE Model was used to determine the rating factors for the LC-5 test truck and the standard TriAxle truck. The ratings were determined by limiting the stress in concrete and reinforcing steel to allowable values. So, the load factors  $A_1$  and  $A_2$  for the rating equation (Equation 2) are 1.0. The allowable unit stresses are given in Table 5. The ratings were determined by applying the full dead load to the FE model and then incrementally increasing the truck weight until the stress in concrete or steel reached the allowable value. The truck weight at that point is represented by  $RF(1+I)L$  as shown in Figure 9.

AASHTO Manual [1] specify allowable stresses for reinforcing steel and compression due to bending in concrete. These stresses were used to perform rating calculations (Table 5). The dynamic allowance was taken as 0.3 to achieve the conservative values of the ratings.

The model was used to investigate the stresses in concrete and reinforcing bars for various load configurations.

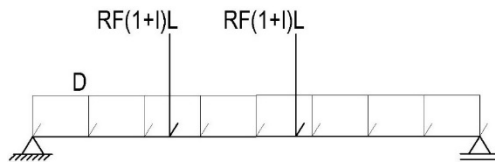


Fig. 9. Scheme of load application in FEM

Table 5. Allowable unit stresses

	Stresses [MPa]	
	Inventory Level	Operating Level
Reinforcing bars	124.00	172.00
Concrete in compression	5.50	8.30

To determine the rating factor of the bridge, the FE model was loaded with dead load and a fraction of the live load which was incrementally increased as described above. These analyses were performed for two live load configurations, two ALDOT’s LC-5 trucks (Fig. 5) side-by-side and two side-by-side TriAxle vehicles (Fig. 4). Vehicles were placed at the most critical longitudinal and transverse locations, resulting in the highest stresses and compared with allowable bending unit stresses in concrete and steel. It turned out that stresses in concrete control, therefore only ratings due to concrete in bending are considered. The live load multiplier,  $RF(1+I)$ , was read at concrete stresses corresponding to inventory and operating level of rating and divided by dynamic allowance,  $(1+I)$ . Such approach gives the most realistic rating factors determined from 3D FEM. Table 6 shows calculations performed for the two truck configurations.

Table 6. Allowable stress ratings.

Vehicle	Live Load Multiplier, $RF(1+I)$		Operating RF	Inventory RF
	Operating Level	Inventory Level		
2×LC-5	5.08	3.74	3.91	2.88
2×TriAxle	5.43	4.15	4.18	3.19

Resulting values of rating factors are higher than those calculated using the AASHTO procedure (Table 3). The ratios of rating factor obtained from FEM and AASHTO procedure are shown in Fig. 10.

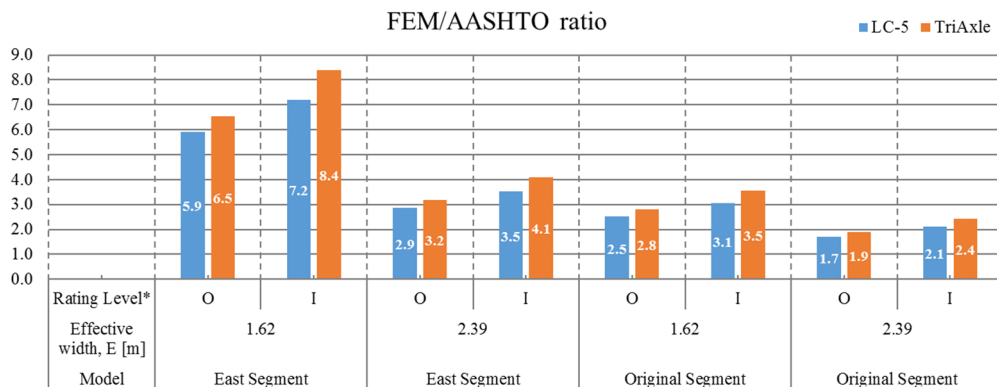


Fig. 10. Resulting ratings comparison – FEM to AASHTO.

All the rating factors determined from FEM are more than 70% above those determined by AASHTO procedure. Comparisons shown in Fig. 10 support a recommendation for a model for permit loads for use by ALDOT having the characteristics of the Original Segment with an effective width equal to 1/4 of the bridge width, 2.39 m.

## 9. Conclusions

A 100 year old reinforced concrete slab bridge was considered to determine and verify the load carrying capacity. As documentation is not available, the bridge was subjected to field testing and advanced analytical procedures. The paper provides a summary of the field measurements using GPR, UPV testing device, ACCM, core tests and live load tests. The FEM confirmed an overall good correlation between the analytically predicted and measured values of strain and deflection. It was found that the rating factors determined using the FE Model are much higher than those calculated using the AASHTO procedure, even though they are conservative. In summary it is concluded that the considered bridge is in good condition and can continue to carry regular traffic without any restrictions. The calculated rating factors can be used in evaluation of bridges for permit loads. In permit load evaluation, the effective width of the slab can be taken as 1/4 of the total width of the bridge.

## Acknowledgments

The research reported in this paper was conducted by authors being part of Highway Research Center at Auburn University, with the sponsorship of the Alabama Department of Transportation. Special thanks are due to Golpar Garmestani, Marek Kolodziejczyk, Anjan Ramesh Babu and Victor Aguilar who are graduate students also involved in this research project.

## References

1. AASHTO: Manual for bridge evaluation, 2nd Ed., Farmington Hills, MI, 2011.
2. State Highway Commission of Alabama. Montgomery, Alabama, USA, Brown Printing Co., 1916.
3. AASHTO: Standard specifications for highway bridges. 17th Ed. Farmington Hills, MI, 2002.
4. ABAQUS: Abaqus analysis user's manual, Version 6.14, Dassault Systèmes, 2014.
5. Kmiecik P., Kamiński M.: Modelling of reinforced concrete structures and composite structures with concrete strength degradation taken into consideration. Archives of Civil and Mechanical Engineering, Vol. XI, No. 3, pp. 623–636, 2011.
6. American Concrete Institute: ACI 318–14 Building Code Requirements for Structural Concrete and Commentary, 2014.
7. European Committee for Standardization: EN 1992-1-1: Design of concrete structures – Part 1–1: General rules and rules for buildings, 2004.
8. Desayi P. and Kirshnan S.: Equations for the stress-strain curve of concrete, ACI Materials Journal 61, pp. 345–350, 1964.
9. Wang T., Hsu T.T.C: Nonlinear finite element analysis of concrete structures using new constitutive models, Computers and Structures, Vol. 79, Iss. 32, pp. 2781–2791, 2001.
10. EDR 48: Evaluation of Reinforcing Bars in Old Reinforced Concrete Structures, CRSI, 2001.